

ChemComm

Accepted Manuscript



This is an *Accepted Manuscript*, which has been through the Royal Society of Chemistry peer review process and has been accepted for publication.

Accepted Manuscripts are published online shortly after acceptance, before technical editing, formatting and proof reading. Using this free service, authors can make their results available to the community, in citable form, before we publish the edited article. We will replace this *Accepted Manuscript* with the edited and formatted *Advance Article* as soon as it is available.

You can find more information about *Accepted Manuscripts* in the [Information for Authors](#).

Please note that technical editing may introduce minor changes to the text and/or graphics, which may alter content. The journal's standard [Terms & Conditions](#) and the [Ethical guidelines](#) still apply. In no event shall the Royal Society of Chemistry be held responsible for any errors or omissions in this *Accepted Manuscript* or any consequences arising from the use of any information it contains.



ChemComm

COMMUNICATION

Facile fabrication of magnetite nanoparticles and their enhanced catalytic performance in Fischer–Tropsch synthesis†

Received 00th January 20xx,
Accepted 00th January 20xx

Shenke Zheng,^{abc} Jiaqiang Sun,^b Dechen Song,^c Zheng Chen,^{ab} and Jiangang Chen^{*a}

DOI: 10.1039/x0xx00000x

www.rsc.org/chemcomm

Uniform and crystalline magnetite nanoparticles are facilely fabricated and utilized as an efficient catalyst for Fischer–Tropsch synthesis (FTS). The catalyst exhibits a high and stable activity with low methane selectivity, attributed to its remarkable structural and chemical stability at the realistic conditions of FTS.

Magnetite nanoparticles (NPs) are of great interest for their wide applications in many different fields, such as biomedicine,¹ magnetic resonance imaging (MRI),² magnetic separation and catalysis.³ Tremendous efforts have been devoted to fabricating active NPs catalysts and exploring their catalytic properties for scientific and industrial perspectives.⁴ Due to its low cost, high water-gas shift (WGS) activity and flexible operation, iron-based catalysts are widely applied in Fischer–Tropsch synthesis (FTS),⁵ a catalytic process for the production of ultraclean liquid fuels and valuable chemicals from natural gas, coal, or biomass.⁶ Previous research reveals that the physical and chemical properties of active NPs, such as particle size,⁷ size distribution,⁸ morphology,⁹ strong metal-support interactions (SMSI) and chemical composition,¹⁰ show significant influences on the catalytic performance of iron-based FTS catalysts. Therefore, it is of great importance to fabricate iron-based NPs with unique properties for the rational design and large-scale application of highly efficient FTS catalysts. However, problematic issues are often encountered in practice, such as delicate controls,¹¹ laborious or time consuming steps,¹² size non-uniformity,¹³ and undesired impurities (*e.g.*, Cl, Br, B) which potentially cause unpredictable impacts on the catalytic properties.^{5a,14} Meanwhile, the undesirable gradual phase transformation from active carbide phase to inactive magnetite and the synchronous particle agglomeration and growth of iron-based NPs catalysts

are commonly observed during the initial period of FTS reaction, resulting in a rapid deactivation and deteriorated selectivity.^{5a,12,15} In addition, of particular note is the significantly high methane yields of iron-based NPs catalysts, which undermines the economic efficiency of FTS technology.¹⁶

Herein, we report a facile and efficient route to synthesize highly crystalline magnetite NPs with controlled size and chemical composition, conveniently used as a catalyst precursor for FTS in slurry operation. The synthesis procedure is based on solvothermal synthesis,¹⁷ partially modified in order to tune the particle size and enhance size uniformity (see the ESI† for more details). A series of well-defined NPs with an average size less than 10 nm, a critical size range for a structure-sensitive reaction such as FTS,^{7,18} were fabricated respectively, with good reproducibility. In a typical experiment, iron(III) acetylacetonate (Fe(acac)₃) was dissolved in benzyl alcohol under vigorous stirring, then gradually heated to 190 °C and held for 2 h in air atmosphere. Finally, the resultant dark colloidal solution containing magnetite NPs with an average size of 7 nm was cooled to room temperature and served as a catalyst precursor.

The peaks at 35.4° and 62.5° in X-ray diffraction (XRD) patterns are assigned to the (311) and (440) planes of magnetite (Fe₃O₄), respectively (Fig. 1a). The relatively broad diffraction peaks indicate a very small crystallite size of the NPs. The phase composition of as-synthesized NPs is further confirmed to be Fe₃O₄ by other characterizations (see the ESI† for more details and Fig. S3, ESI†), consistent with previous reports.¹⁷

The transmission electron microscopy (TEM) images show that most of the Fe₃O₄ NPs are well dispersed with near-spherical shape and have a uniform size of *ca.* 2.5 nm, 4 nm, 7 nm and 10 nm, respectively (Fig. 1b–e). It is noticed that the particle size distribution (PSD) become broader with increasing size of NPs. High-resolution TEM (HRTEM) images show detailed structure of the as-synthesized NPs with high crystallinity and well-defined atomic planes (Fig. 1f–g). The planar *d* (2.96±0.05 Å and 2.53±0.05 Å) of these particles is consistent with the (220) and (311) planes of Fe₃O₄ respectively.

The catalytic performance of active NPs are dramatically affected by the existence of SMSI,^{10b,10c} and hampered due to the

^a State Key Laboratory of Coal Conversion, Institute of Coal Chemistry, Chinese Academy of Sciences, Taiyuan, 030001, China. E-mail: chenjjg@sxicc.ac.cn

^b Graduate University of Chinese Academy of Science, Beijing, 100039, China

^c State Key Laboratory of Biomass Thermal Chemistry Technology, Sunshine Kaidi New Energy Group Co., Ltd. Wuhan, 430223, China

† Electronic supplementary information (ESI) available: Experimental details, Table of reagents usage and catalytic performance comparison (Tables S1–S2 and Fig. S7), characterization techniques such as GC-MS, H₂-TPR, TEM and photographs of magnetic separation (Fig. S1–S6). See DOI: 10.1039/c000000x/

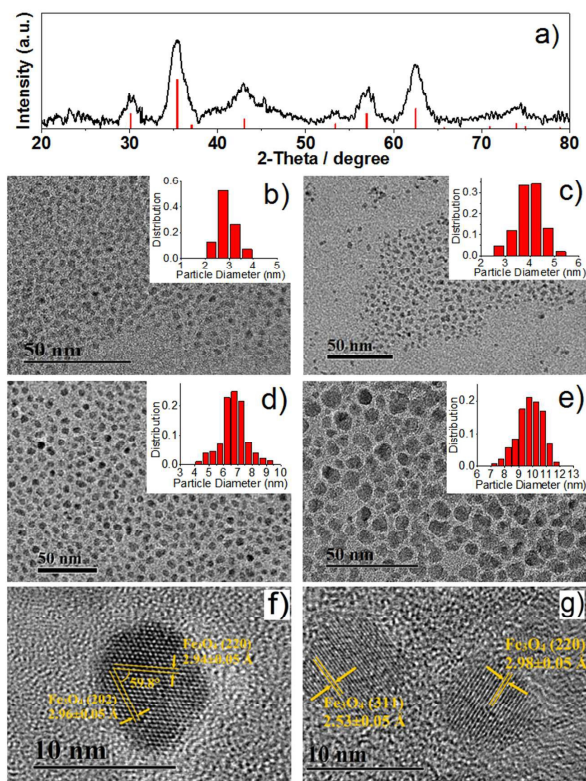


Fig. 1 Structural characterization of as-synthesized iron oxide NPs: (a) normalized XRD patterns of Fe_3O_4 NPs (JCPDS 19-0629); (b-e) TEM image of NPs of increasing size (2.5, 4, 7 and 10 nm), the insets show the corresponding size distribution, calculated from the statistical TEM data over 250 particles for each sample; (f-g) HRTEM image of NPs with size of ca. 7 nm.

lack of three-dimensional freedom of NPs immobilized on supports.¹⁹ Therefore, the performance evaluation of the iron-based NPs catalyst with mean diameter of 7 nm was conducted in the absence of any support materials or isolation of other NPs (e.g., Al_2O_3 , SiO_2) immediately after *in situ* synthesis under industrially relevant conditions. The detailed activation and evaluation procedures for NPs catalyst are described in the ESI.† The variation of the activity (expressed as moles of CO consumed per mole Fe per hour, $\text{mol}_{\text{CO}}/\text{mol}_{\text{Fe}}/\text{h}$), calculated based on CO conversion, and product selectivity (expressed as Cmol% on a carbon atom basis) with time-on-stream (TOS) are shown in Fig. 2. The activity of NPs catalyst reaches a nearly constant value of ca. $2.9 \text{ mol}_{\text{CO}}/\text{mol}_{\text{Fe}}/\text{h}$ after the first 30 h of reaction (Fig. 2a), which equals to about 40 % of CO conversion. The selectivity of light hydrocarbon shows a similar tendency, reaches steady-state values of 2.5 % and 12.6 % for methane and $\text{C}_2\text{-C}_4$ respectively after 20 h, and the selectivity for C_5+ products is around 85 % (Fig. 2b). The NPs catalyst shows enhanced catalytic performance in terms of high and stable activity with unprecedentedly low methane selectivity (Table S2, ESI†). And compared with the previous reports,^{5a,15} the activity of NPs catalyst in current study increases steadily, rather than decreases sharply, during the initial period of reaction.

After reaction, structure and phase composition of the spent catalyst sample were further characterized. The peaks of XRD

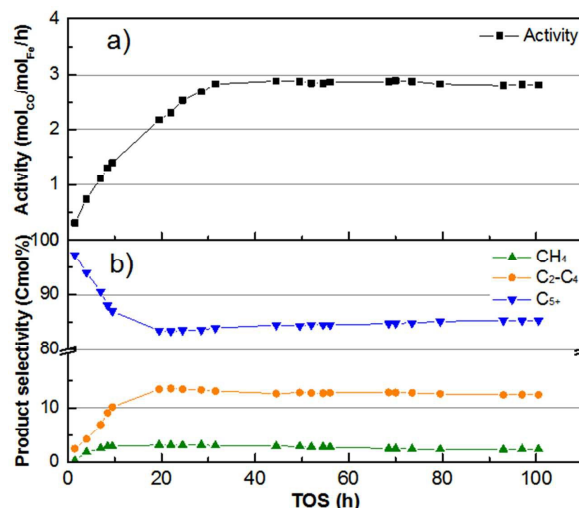


Fig. 2 (a) NPs catalyst activity and (b) hydrocarbon products selectivity with time-on-stream. Reaction conditions: 250°C , 2.0 MPa, $\text{H}_2/\text{CO}=2(\text{v/v})$, gas hourly space velocity at $10 \text{ L/h/g}_{\text{cata}}$.

patterns (Fig. 3a) are apparently sharper than that of the as-synthesized NPs (Fig. 1a), suggesting a larger crystallite size of NPs catalyst. The TEM images show loose aggregates of partly overlapped particles with a primary size ranging from 10 to 14 nm (Fig. 3b). However, it is noteworthy that the PSD of NPs catalyst both after CO pre-treatment (Fig. S4, ESI†) and reaction (Fig. 3b) are much the same. Though a very small number of large-sized particles (< 2 % in number) with diameters up to 100 nm appear in TEM images (Fig. S5), particles of intermediate size between 20 and 80 nm are barely observed, implying that most of the individual particles maintain their structure and cease to grow during 100 h on stream. After reaction, Hägg carbide (Fe_5C_2 , JCPDS 51-0997), known as an active phase for FTS,^{5a,20} appears in the XRD patterns (Fig. 3a, sharp reflection at $43\text{--}44^\circ$), while the peaks (very weak reflection at 35.5°) assigned to magnetite are negligible (3.9 wt% fraction of iron phases as determined by Rietveld refinement). Furthermore, typical HRTEM images of the catalyst particle present well-defined

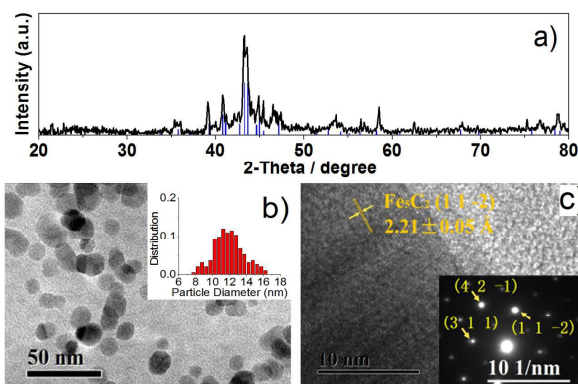


Fig. 3 Structural characterization of the spent NPs catalyst after reaction for 100 h: (a) normalized XRD patterns of Fe_5C_2 (JCPDS 51-0997); (b) TEM image of NPs catalyst, the inset show the corresponding size distribution, calculated from the statistical TEM data over 200 particles; (c) Typical HRTEM images of the large-sized particle and its SAED pattern (inset).

lattice planes with planar d of $2.21 \pm 0.05 \text{ \AA}$ (Fig. 3c) and $2.06 \pm 0.05 \text{ \AA}$ (Fig. S6, ESI[†]), consistent with the (11 $\bar{2}$) and (510) planes of Fe₃C₂ respectively. Therefore, the possibility of amorphous Fe₃O₄ phase in the spent catalyst can be excluded. The corresponding selected area electron diffraction (SAED) patterns of the large-sized particle are indexed to the (311), (42 $\bar{1}$) and (11 $\bar{2}$) diffraction planes of Fe₃C₂, respectively, which further confirms the high crystallinity of NPs catalyst (inset of Fig. 3c). Presumably, catalyst particles assemble to form loosely attached aggregates and then quickly transform into the bulk-like crystals,²¹ during which phase transformation is not involved. Unambiguously, Fe₃C₂ is the predominant phase of NPs catalyst, and re-oxidation under reaction condition is hardly observed in the current study. It should be noted that Fe-based catalysts are easily oxidized upon exposure to air,^{5b} accurate *ex situ* characterization of surface oxidation and carbon deposition, which may play important roles in catalytic properties, could not be experimentally conducted under current investigation.

To the best of our knowledge, unpromoted and unsupported iron-based NPs catalysts in previous literatures were generally instable during the initial period of reaction, the active iron carbide phase was susceptible to water, produced upon exposure to syngas, which caused the gradual and irreversible re-oxidation of iron carbide to magnetite.^{5a,12,15} As a result, the activity of the catalysts usually dropped strikingly at first and stayed at a low level afterward. Re-oxidation under reaction condition was observed on different types of iron-based NPs catalysts, such as amorphous iron ultrafine particles prepared by liquid phase reduction method,^{15b} commercial iron oxide NPs catalysts,^{15c,15d} and more recently, Fe₂O₃ NPs fabricated by thermal decomposition,¹² and iron carbide NPs synthesized by plasma-spraying technology and wet-chemical route respectively.^{5a,15a} It was reported that about 50 % of iron was found to be present as Fe₃O₄ only after the first 30 h of reaction and its fraction continued to increase with TOS for iron-based NPs catalyst without any promoter, and concluded that re-oxidation and the growth of NPs, another factor contributed to the deteriorated performance, occurred either successively or simultaneously.^{15d} However, in the current study, the catalytic performance of NPs catalyst was quite remarkable, exhibiting high activity and long-term stability with unprecedentedly low methane selectivity. Meanwhile, the individual particles of NPs catalyst maintained their size and re-oxidation of active phase was hardly observed during FTS reaction.

The macroscopic catalytic performance depends on the microcosmic structure and chemical composition of catalysts.²² Thus, it is reasonable to attribute the remarkable performances of the NPs catalyst to its distinctively stable structure and chemical composition at the realistic reaction conditions.

In summary, a facile and efficient route has been developed to address the practical preparation of highly crystalline magnetite NPs in large scale with well controlled particle size, size distribution and chemical composition. The obtained NPs are utilized as a FTS catalyst precursor in slurry phase operation under industrially relevant conditions, exhibiting an enhanced catalytic performance with a high activity, long-term stability

and suppressed formation of methane, attributed to its unusual stable structure and chemical composition. It is expected that this work can promote scalable and cost-affordable fabrication of iron-based NPs and provide new clues to develop highly efficient FTS catalysts for both scientific researches and potential industrial applications.

We gratefully acknowledge the financial support from the National Natural Science Foundation of China (no. 21373254), the autonomous research project of SKLCC (no. 2014BWZ003), and the support from the State Key Laboratory of Biomass Thermal Chemistry Technology (Wuhan) is also appreciated.

Notes and references

- L. H. Reddy, J. L. Arias, J. Nicolas and P. Couvreur, *Chem. Rev.*, 2012, **112**, 5818.
- H. Yang, C. Zhang, X. Shi, H. Hu, X. Du, Y. Fang, Y. Ma, H. Wu and S. Yang, *Biomaterials*, 2010, **31**, 3667.
- (a) M. B. Gawande, P. S. Branco and R. S. Varma, *Chem. Soc. Rev.*, 2013, **42**, 3371; (b) A. H. Lu, E. L. Salabas and F. Schüth, *Angew. Chem. Int. Ed.*, 2007, **46**, 1222.
- (a) Y. Li and W. Shen, *Chem. Soc. Rev.*, 2014, **43**, 1543; (b) Y. Wu, D. Wang and Y. Li, *Chem. Soc. Rev.*, 2014, **43**, 2112; (c) B. Roldan Cuenya, *Acc. Chem. Res.*, 2012, **46**, 1682.
- (a) C. Yang, H. Zhao, Y. Hou and D. Ma, *JACS*, 2012, **134**, 15814; (b) E. de Smit and B. M. Weckhuysen, *Chem. Soc. Rev.*, 2008, **37**, 2758.
- (a) G. P. Van Der Laan and A. A. C. M. Beenackers, *Catalysis Reviews*, 1999, **41**, 255; (b) P. R. Chadeesingh, in *The Biofuels Handbook*, The Royal Society of Chemistry, 2011, pp. 476.
- H. M. Torres Galvis, J. H. Bitter, T. Davidian, M. Ruitenbeek, A. I. Dugulan and K. P. de Jong, *JACS*, 2012, **134**, 16207.
- P. Munnik, P. E. de Jongh and K. P. de Jong, *JACS*, 2014, **136**, 7333.
- J. Sun, S. Zheng, K. Zhang, D. Song, Y. Liu, X. Sun and J. Chen, *Journal of Materials Chemistry A*, 2014, **2**, 13116.
- (a) C. Wang, H. Zhao, H. Wang, L. Liu, C. Xiao and D. Ma, *Catal. Today*, 2012, **183**, 143; (b) S. O. Moussa, L. S. Panchakarla, M. Q. Ho and M. S. El-Shall, *ACS Catalysis*, 2013, **3**, 535; (c) R. P. Mogorosi, N. Fischer, M. Claeys and E. van Steen, *J. Catal.*, 2012, **289**, 140.
- (a) V. R. Calderone, N. R. Shiju, D. Curulla-Ferré, S. Chambrey, A. Khodakov, A. Rose, J. Thiessen, A. Jess and G. Rothenberg, *Angew. Chem. Int. Ed.*, 2013, **52**, 4397; (b) A. Nakhaei Pour and M. R. Housaindokht, *Journal of Industrial and Engineering Chemistry*, 2014, **20**, 591.
- H. Dong, M. Xie, J. Xu, M. Li, L. Peng, X. Guo and W. Ding, *Chem. Commun.*, 2011, **47**, 4019.
- X. B. Fan, Z. Y. Tao, C. X. Xiao, F. Liu and Y. Kou, *Green Chemistry*, 2010, **12**, 795.
- (a) X. Cheng, B. Wu, Y. Yang, H. Xiang and Y. Li, *J. Mol. Catal. A: Chem.*, 2010, **329**, 103; (b) J. Tu, M. Ding, Y. Zhang, Y. Li, T. Wang, L. Ma, C. Wang and X. Li, *Catal. Commun.*, 2015, **59**, 211.
- (a) J. Blanchard, N. Abatzoglou, R. Eslahpazir-Esfandabadi and F. Gitzhofer, *Industrial & Engineering Chemistry Research*, 2010, **49**, 6948; (b) H. Itoh, H. Hosaka, T. Ono and E. Kikuchi, *Applied Catalysis*, 1988, **40**, 53; (c) D. Mahajan, P. Gütllich and U. Stumm, *Catal. Commun.*, 2003, **4**, 101; (d) A. Sarkar, D. Seth, A. Dozier, J. Neathery, H. Hamdeh and B. Davis, *Catal. Lett.*, 2007, **117**, 1.
- T. H. Pham, Y. Qi, J. Yang, X. Duan, G. Qian, X. Zhou, D. Chen and W. Yuan, *ACS Catalysis*, 2015, **5**, 2203.
- N. Pinna, S. Grancharov, P. Beato, P. Bonville, M. Antonietti and M. Niederberger, *Chem. Mater.*, 2005, **17**, 3044.
- A. Nakhaei Pour and M. R. Housaindokht, *Journal of Natural Gas Science and Engineering*, 2013, **14**, 204.
- (a) S. N. Khadzhiev, A. S. Lyadov, M. V. Krylova and A. Y. Krylova, *Petroleum Chemistry*, 2011, **51**, 24; (b) C. Xiao, Z. Cai, T. Wang, Y. Kou and N. Yan, *Angew. Chem. Int. Ed.*, 2008, **47**, 746.
- M. O. Ozbek and J. W. Niemantsverdriet, *J. Catal.*, 2014, **317**, 158.
- Z. Zhuang, F. Huang, Z. Lin and H. Zhang, *JACS*, 2012, **134**, 16228.
- F. Tao, L. Nguyen and S. Zhang, in *Metal Nanoparticles for Catalysis: Advances and Applications*, The Royal Society of Chemistry, 2014.